

Off-diagonal electron-phonon coupling effects on two-level system dynamicsLeonard Ruocco¹,* Mona Berciu, and Jeff F. Young*Department of Physics and Astronomy, University of British Columbia, Vancouver, British Columbia, V6T 1Z1 Canada
Stewart Blusson Quantum Matter Institute, University of British Columbia, Vancouver, British Columbia, V6T 1Z4 Canada*

(Received 12 January 2022; revised 3 June 2022; accepted 6 June 2022; published 28 June 2022)

Electromagnetically coupled two-level systems play a central role in several condensed matter components being considered for quantum information processing applications. If the states couple to phonon excitations, their electromagnetic response is altered via phonon-assisted transitions and lifetime broadening. The former has been treated extensively for a number of specific two-level systems (e.g., excitons in artificial quantum dots, localized states associated with impurities or defects, etc.), but the latter has received less attention. Here we study a microscopic model of the dipole transition of a two-level system under the influence of both diagonal and nondiagonal interactions with a bath of phonons. Our results capture both the influence of the frequency distribution of phonons on the relative spectral weight of the zero-phonon transition and the phonon sidebands, and the broadening of the zero-phonon line due to nondiagonal electron-phonon coupling. We use a formalism that includes non-Markovian effects related to the feedback mechanism between the two-level system and the phonon bath. For simplified forms of the phonon spectral functions we provide analytical expressions up to second order in the coupling strength that demonstrate the importance of including both forms of electron-phonon coupling in studies of these systems. Our formalism can be generalized to higher orders of coupling and for realistic phonon spectral functions.

DOI: [10.1103/PhysRevB.105.214310](https://doi.org/10.1103/PhysRevB.105.214310)**I. INTRODUCTION**

Some defect centers in dielectric environments are characterized by localized electronic states that are known to exhibit remarkably long coherence times [1–3], making them attractive as quantum information processing components. However, direct electronic coupling of the long-lived defect states, towards the purpose of quantum-gate implementation, is challenging due to the requirement for them to be in close proximity (within a few nanometers). “Spin-photon” interfaces that access the long-lived states via electromagnetic transitions to higher lying excited states have been proposed to solve this problem, based on the use of cavity quantum electrodynamics [4]. However, engineering spin qubits with favorable excited-state optical or microwave transition characteristics, as well as effectively accessing and utilizing the dipole-coupled states, remains a challenge, in part because of the presence of electron-phonon coupling in the solid-state lattice [5].

Vibrations in the host lattice manifest as both continuous acoustic and discrete Einstein optical phonon modes that can couple to the defect states, affecting their electromagnetic coupling properties [6]. This coupling generally poses a hurdle to developing high-quality single-photon sources, and more generally spin-photon interfaces, which are necessary for the development of photonic-based, fault tolerant quantum-computing networks [5,7]. Understanding the role of electron-phonon interactions with the goal of mitigating their

adverse effects, is therefore paramount for advancing the field of optically coupled, defect-based quantum computing.

The most commonly studied model of electron-phonon interactions involving localized dipole transitions utilizes Holstein (diagonal) coupling [8], where phonons modulate (dress) the energy levels constituting the optical transition. This form of electron-phonon interactions has been extensively studied in the context of spin-photon interfaces [9,10], quantum dot single photon sources [11], and more generally in terms of spin-boson systems [12]. The other, Peierls (nondiagonal) form of electron-phonon coupling [13] arises because the phonons also modulate the hopping integrals (tunneling) between these energy levels. In solids, the Peierls coupling has been shown to result in polarons whose properties are qualitatively different from those of Holstein polarons [14–17]. While it has been included in calculations pertinent to defect spin qubits via dynamical symmetry breaking [18], the Peierls coupling is commonly neglected in this context because of the complications it poses.

In this work we use a generic microscopic model at zero temperature that captures the influence of both diagonal and nondiagonal electron-phonon coupling on the absorption/emission properties of a two-level electronic dipole transition within the band gap of a host dielectric (see Appendix A for more details). This model captures the shape of the phonon sideband contribution to the spectrum, the relative spectral strength of the zero-phonon line (ZPL), and the ZPL linewidth broadening which is due solely to the Peierls coupling. While previous works have used Fermi’s golden rule (FGR) to study the effects of both forms of coupling separately on the longitudinal spin-relaxation time of donor-bound electrons in direct band-gap semiconductors [19], here

*Corresponding author: leon.ruocco@ubc.ca

both forms of coupling are considered simultaneously, and through the use of Greens functions we are able to calculate the entire spectral response of the system. The methods used in this work also allow us to go beyond FGR and consider non-Markovian effects which retain feedback mechanisms between the defect and phonon bath.

Other works have explored the effect of virtual phonons on dephasing, incorporating higher-order diagonal couplings which are quadratic in phonon operators [20]. While ZPL linewidth broadening has been predicted in this case, this effect is entirely temperature dependent. Conversely, our study focuses on a zero-temperature model where quantum fluctuations are entirely responsible for all predicted broadening.

The basic formulation is valid for arbitrary coupling strengths, but we provide specific analytic results up to second order in the coupling strength for a range of parametrized phonon spectral functions. A comparison is also made to experimental results reported for a microwave transition associated with the phosphorus (P) impurity in silicon (Si) [21], and for a midinfrared transition associated with singly ionized selenium (Se) impurities, also in silicon [1,22]. While the analytic form of the phonon spectral functions used in the present work prohibit a quantitative comparison with experimental results, the parametric dependence of the model predictions for P in silicon suggest that higher than first order terms are likely playing a role in the ZPL linewidth associated with Peierls coupling. For ionized Se, the contrasts in model versus experimental phonon sideband spectra and the relative spectral weight of the ZPL transition, provide strong motivation for numerically extending this work to higher order coupling, using more realistic phonon spectral functions.

The paper is structured as follows: Section II describes our model and Sec. III explains how we calculate its absorption/emission spectrum. Section IV shows representative results and Sec. V contains a summary and discussions. Some technical details are relegated to Appendices.

II. THE MODEL

We model the dipole transition as a two-level system (TLS) spanning the basis $\{|1\rangle, |2\rangle\}$, coupled to a phonon bath representing both the acoustic and the optical phonon modes of the host semiconductor [6,23]. Our Hamiltonian is

$$H = \frac{1}{2}\epsilon\sigma_z + \frac{1}{2}(\sigma_z + \zeta\sigma_x) \sum_q \lambda_q (b_q^\dagger + b_q) + H_{\text{ph}}, \quad (1)$$

where ϵ is the transition energy, $\sigma_z = |1\rangle\langle 1| - |2\rangle\langle 2|$, $\sigma_x = |1\rangle\langle 2| + |2\rangle\langle 1|$, and b_q^\dagger, b_q are the bosonic creation and annihilation operators, respectively, for a phonon mode q of energy ω_q . The phonon bath is described by $H_{\text{ph}} = \sum_q \omega_q b_q^\dagger b_q$ (we set $\hbar = 1$).

Our Hamiltonian includes both types of coupling to the phonon bath [24]. The ‘‘diagonal’’ Holstein term, of strength λ_q , couples the phonon displacement operator $b_q + b_q^\dagger$ to the σ_z spin degree of freedom, and describes a fluctuating dipole-polarization term.

The ‘‘nondiagonal’’ Peierls term couples the phonons to σ_x , describing a tunneling matrix element modulated by phonon emission and absorption. As mentioned, this term is usually ignored because of the complications it introduces, even

though it is generally present in real systems. Here we assume that its magnitude $\zeta\lambda_q$ is proportional to that of the diagonal coupling, with ζ being a small, dimensionless number. This proportionality is simply a convenient approximation that allows us to deal with this Peierls coupling relatively easily, to weigh its importance.

In realistic models, one expects the couplings to differ more significantly and if one was to relax the assumption of proportional couplings, then there would be no *a priori* reason to exclude an inhomogeneous coupling to σ_y also. However, doing this would significantly complicate the treatment, therefore the degree to which this inhomogeneity might suppress the effects of a nondiagonal coupling remains to be seen [25]. Nevertheless, the results for our simpler model show that it is necessary to deal with this complication instead of ignoring the off-diagonal term, as done previously.

To proceed we turn to the ‘‘polaron frame’’ by making use of the following unitary transformation:

$$\tilde{U} = e^{-S}, \quad S = \frac{\sigma_z + \zeta\sigma_x}{2} \sum_q u_q (b_q - b_q^\dagger), \quad (2)$$

where $u_q = \lambda_q/\omega_q$. Performing the transformation $H \rightarrow \tilde{U}H\tilde{U}^\dagger \equiv \tilde{H}$, and ignoring a constant energy shift as well as states with multiple excitations [17], produces

$$\tilde{H} = \frac{1}{2}\hat{\epsilon}\sigma_z + \frac{1}{2}\hat{K}_-\sigma_+ + \frac{1}{2}\hat{K}_+\sigma_- + H_{\text{ph}}, \quad (3)$$

where the transformed on-site energy $\hat{\epsilon} = \epsilon_\zeta - \delta\hat{\epsilon}$ and transformed tunneling energies \hat{K}_\pm are functions of the boson operators:

$$\epsilon_\zeta = \epsilon + \frac{\zeta^2\epsilon}{1 + \zeta^2}, \quad \delta\hat{\epsilon} = \frac{\zeta^2\epsilon}{1 + \zeta^2} \cosh(\hat{\phi}_\zeta), \quad (4)$$

and

$$\hat{K}_\pm = \frac{\zeta\epsilon}{1 + \zeta^2} (\cosh(\hat{\phi}_\zeta) - 1) \pm \frac{\zeta\epsilon}{\sqrt{1 + \zeta^2}} \sinh(\hat{\phi}_\zeta), \quad (5)$$

where

$$\hat{\phi}_\zeta = \sqrt{1 + \zeta^2} \sum_q u_q (b_q - b_q^\dagger).$$

In order to facilitate further analysis, we move to the interaction picture, separating the Hamiltonian $\tilde{H} = \tilde{H}_0 + \tilde{H}'$ into its free part $\tilde{H}_0 = H_B$ and its interaction part

$$\tilde{H}' = \frac{1}{2}\hat{\epsilon}(t)\sigma_z + \frac{1}{2}\hat{K}_-(t)\sigma_+ + \frac{1}{2}\hat{K}_+(t)\sigma_-. \quad (6)$$

The phonon operators now acquire time dependence so that

$$\hat{\phi}_\zeta(t) = \sqrt{1 + \zeta^2} \sum_q u_q (b_q e^{-i\omega_q t} - b_q^\dagger e^{i\omega_q t}). \quad (7)$$

III. SINGLE DEFECT FLUORESCENCE EMISSION SPECTRUM

In the interest of modeling the experimentally determined emission spectra from single-photon emitters [22], we study the fluorescence emission determined from the spectral intensity radiated per unit solid angle [18,26]

$$\frac{dI}{d\Omega} = \frac{\omega_0^4}{8\pi^2 c^3} |(\mathbf{n} \times \mathbf{d}) \times \mathbf{n}|^2 S(\xi), \quad (8)$$

where \mathbf{d} is the dipole vector, \mathbf{n} is the corresponding directional unitary vector, and ω_0 is the frequency of incident radiation. The frequency dependence of emitted radiation is determined by the emission spectrum

$$S(\xi) = \text{Re} \int_0^\infty dt e^{i\xi t} \langle \sigma_-(t) \sigma_+(0) \rangle_{\text{ph}}, \quad (9)$$

where the average $\langle \cdots \rangle_{\text{ph}} = \text{tr}_{\text{ph}}(\rho_{\text{ph}} \cdots)$ denotes the average over the phonon bath. Assuming the phonon bath to be in thermal equilibrium, and the initial excitation to be instantaneous, we assume zero correlations prior to $t = 0$ such that the full density matrix of the system is initially factorizable $\rho(0) = \rho_S(0) \rho_{\text{ph}}(0)$, where $\rho_S = \text{tr}_{\text{ph}} \rho$ describes the reduced dynamics of the spin and $\rho_{\text{ph}} = \text{tr}_S \rho$ those of the phonon bath only.

As written, the time evolution of Eq. (9) is governed by H . In transforming to the polaron frame, not only do we transform $H \rightarrow \tilde{H}$, but also rotate and dress the spin states $|1\rangle, |2\rangle$ due to the nondiagonal component of the polaron transformation \tilde{U} . The *first approximation* we make is to assume small nondiagonal coupling strengths $\zeta \ll 1$ and discard terms of order $O(\zeta^3)$ and higher. We then find the emission spectrum can be approximated as (see Appendix A for details)

$$S(\xi) \approx \text{Re} \int_0^\infty dt e^{i\xi t} \langle \tilde{G}_{11}^\dagger(t) \tilde{G}_{22}(t) \rangle_{\text{ph}}, \quad (10)$$

written now in terms of operators in the interaction picture. For convenience we define the Green's functions $G_{\alpha\beta}(t) = \langle \tilde{\alpha} | \tilde{U}'(t) | \tilde{\beta} \rangle$, where the unitary time-evolution operator in the interaction picture is the solution to the differential equation $i\partial_t \tilde{U}'(t) = \tilde{H}'(t) \tilde{U}'(t)$. The kets $|\tilde{\alpha}\rangle = e^{-\hat{\phi}_0} |\alpha\rangle$ represent the dressed spin states due to the rotation in Eq. (2).

The next step is to calculate these propagators:

$$\tilde{G}_{\alpha\beta}(t) = \langle \tilde{\alpha} | \exp\left[-i \int_0^t d\tau \tilde{H}'(\tau)\right] | \tilde{\beta} \rangle. \quad (11)$$

The Green's functions can be expressed in their infinite series representation by

$$\begin{aligned} \tilde{G}_{\alpha\beta}(t) &= \sum_{n=0}^{\infty} (-i)^n \int_0^t d\tau_n \cdots \int_0^{\tau_2} d\tau_1 \\ &\times \langle \alpha | e^{\hat{\phi}_0(t)} [\hat{\epsilon}(\tau_n) \sigma_z + \hat{K}_+(\tau_n) \sigma_- + \hat{K}_-(\tau_n) \sigma_+] \cdots \\ &\times [\hat{\epsilon}(\tau_1) \sigma_z + \hat{K}_+(\tau_1) \sigma_- + \hat{K}_-(\tau_1) \sigma_+] e^{-\hat{\phi}_0(0)} | \beta \rangle, \end{aligned} \quad (12)$$

where the expectation value is now taken over the undressed spin states to account for phonon cloud correlations with the initial and final configurations of the bath.

This equation is exact, and correlations are entirely non-local in time and include those created on site and while undergoing a transition. As a result, the number of diagrammatic processes included in (12) is infinite and this series cannot be summed analytically.

At this point we apply our *second approximation* in which we retain only nearest-neighbor (in time) phonon cloud correlations which amounts to a lowest-order cumulant expansion in the bath fluctuations [27]. This approximation has been shown [28,29] to be equivalent to the noninteracting-blip

approximation (NIBA) [12], where coherent spin states are assumed to be short lived. Such an approximation is understood to be valid in the limit of small electron-phonon coupling [30] relative to the characteristic phonon frequency which is the limit we consider here. NIBA therefore amounts to retaining only correlations between successive bath displacements such that the average over the full expansion of operators in Eq. (10) truncates to the average over a product of bath displacement operators [31].

With both approximations in mind it is consistent to retain only nearest-neighbor phonon cloud correlations due to tunneling events—which take the form $\langle \hat{K}_+(t_n) \hat{K}_-(t_{n-1}) \rangle_{\text{ph}}$ —as well as on-site correlations $\langle \delta \hat{\epsilon}(t_n) \rangle_{\text{ph}}$. Note that correlations between tunneling and on-site events are of order $\langle \hat{K}_+(t_n) \delta \hat{\epsilon}(t_{n-1}) \rangle_{\text{ph}} \sim O(\zeta^3)$ and so are suppressed within these approximations.

The correlator in Eq. (10) therefore approximates to

$$\begin{aligned} \langle \tilde{G}_{11}^\dagger(t) \tilde{G}_{22}(t) \rangle_{\text{ph}} &\approx e^{-i\epsilon t} B_0^2 \langle e^{\hat{\phi}_0(t)} e^{-\hat{\phi}_0(0)} \rangle_{\text{ph}} - 2B_0^2 \int_0^t d\tau_2 \\ &\times \int_0^{\tau_2} d\tau_1 e^{-i\epsilon t} \langle \hat{K}_+(\tau_2) \hat{K}_-(\tau_1) \rangle_{\text{ph}}. \end{aligned} \quad (13)$$

The two-point phonon cloud correlation functions can be calculated using a Feynman operator disentangling method [32] (see Appendix C for more details). We find

$$\begin{aligned} \langle \hat{K}_+(t) \hat{K}_-(0) \rangle_{\text{ph}} &= \frac{(\zeta \epsilon)^2 (1 - 2B)}{4(1 + \zeta^2)^2} - \frac{(\zeta \epsilon)^2}{4(1 + \zeta^2)^2} \sinh[\varphi(t)] \\ &+ \frac{(\zeta \epsilon)^2}{4(1 + \zeta^2)^2} \cosh[\varphi(t)] \end{aligned} \quad (14)$$

while $\langle e^{\hat{\phi}_0(t)} e^{-\hat{\phi}_0(0)} \rangle_{\text{ph}} = e^{\varphi_0(t)}$. The phase $\varphi(t)$ is given by

$$\varphi(t) = \sqrt{1 + \zeta^2} \sum_q u_q^2 [n_q (e^{i\omega_q t} - 1) + (1 + n_q) (e^{-i\omega_q t} - 1)] \quad (15)$$

with Bose occupation numbers $n_q = 1/(e^{\beta\omega_q} - 1)$ at temperature $T = 1/(k_B\beta)$ and $\varphi_0(t) = \varphi(t)|_{\zeta=0}$. The Debye-Waller factor $B = \langle e^{\pm\hat{\phi}_\zeta} \rangle_{\text{ph}}$ is linked to the time-independent part of the phase:

$$B = \exp\left[-\sqrt{1 + \zeta^2} \sum_q u_q^2 (1 + 2n_q)\right], \quad (16)$$

and similarly we denote $B_0 = \langle e^{\pm\hat{\phi}_{\zeta=0}} \rangle_{\text{ph}}$. At this point we note that by taking the limit $\zeta \rightarrow 0$, such that the nondiagonal coupling is switched off, we recover the result of Ref. [9] where only diagonal couplings were studied. As we consider only the $T = 0$ K case here, our calculation of the Debye-Waller factor is restricted only to the zero-temperature contribution and can be interpreted as follows. The phonon clouds associated with the two defect states are not identical and therefore their overlap is less than unity. The quantity produced by this overlap is the zero-temperature Debye-Waller factor and physically represents the polarization of the surrounding lattice due to the defect atom, leading to a corresponding reduction in tunneling between the two defect states [33].

These results allow us to formally evaluate the emission spectrum of Eq. (10):

$$S(\xi) = \text{Re}\Upsilon^0(\xi - \epsilon_\zeta - i\eta) + \text{Re}\Upsilon(\epsilon_\zeta - i\eta)\delta(\xi - \epsilon_\zeta - i\eta)^2, \quad (17)$$

where we have applied the convolution theorem and taken the real part of the Fourier transform of the step function $\text{Re}[\theta(\xi)] = \text{Re} \int_0^\infty dt e^{i\xi t} \theta(t) = \pi \delta(\xi)$. We have also analytically continued the frequency $\xi \rightarrow \xi + i\eta$ to include a small phenomenological damping factor η [34]. Furthermore, $\Upsilon^0(\xi) = \int_0^\infty dt e^{-i\xi t} \langle e^{\hat{\phi}_0(t)} e^{-\hat{\phi}_0(0)} \rangle_{\text{ph}}$ defines the Holstein contribution, while the Peierls contribution comes from

$$\Upsilon(\xi) = 2B_0^2 \int_0^\infty dt e^{-i\xi t} \langle \hat{K}_+(t) \hat{K}_-(0) \rangle_{\text{ph}}. \quad (18)$$

To make further progress, we need to model the phonon bath. This is because the phase that appears in the integrand of the above Fourier transforms can be expressed as

$$\varphi(t) = \sqrt{1 + \zeta^2} \int_0^\infty d\omega \frac{J(\omega)}{\omega^2} \left[\coth \frac{\beta\omega}{2} [\cos(\omega t) - 1] - i \sin(\omega t) \right], \quad (19)$$

where the frequency distribution of phonon modes weighted by their coupling strengths to the spin is completely characterized by the spectral density function

$$J(\omega) = \sum_q \lambda_q^2 \delta(\omega - \omega_q). \quad (20)$$

A. Acoustic phonons

It now remains to characterize the bath by choosing a form for $J(\omega)$. Semiconductor substrates usually exhibit deformation potential coupling to acoustic phonon modes, with an expression for λ_q listed in Appendix B. Given that this form of coupling is dominated by the long-wavelength portion of the phonon dispersion [32], we assume a linear Debye approximation for the acoustic phonon branches $\omega_q = v|q|$, where v is either a longitudinal or transverse sound velocity, depending on the branch. Turning the discrete sum over q into an integral and summing over one longitudinal and two transverse acoustic branches (see Appendix B for details), we recover the well known cubic form for the spectral density $J_{\text{ac}}(\omega) = \gamma_{\text{ac}}(\omega^3/\omega_c^2)$, where γ_{ac} is a dimensionless acoustic phonon coupling strength and ω_c is the ‘‘characteristic’’ acoustic phonon frequency scale, related to material constants.

In real physical systems, there are upper limits to the phonon frequencies and furthermore, the Debye approximation of a linear dispersion breaks down near the Brillouin zone boundary. Therefore, the phonon density of states must be skewed towards the low frequency portion of the dispersion and fall off rapidly as we approach the K point. To account for this we introduce a standard cutoff [27]:

$$J_{\text{ac}}(\omega) = \gamma_{\text{ac}} \frac{\omega^3}{\omega_c^2} e^{-\frac{\omega}{\omega_c}}. \quad (21)$$

In Fig. 1 we plot $J_{\text{ac}}(\omega)$ for several values of the parameter ω_c . We note that the distribution of acoustic phonon modes

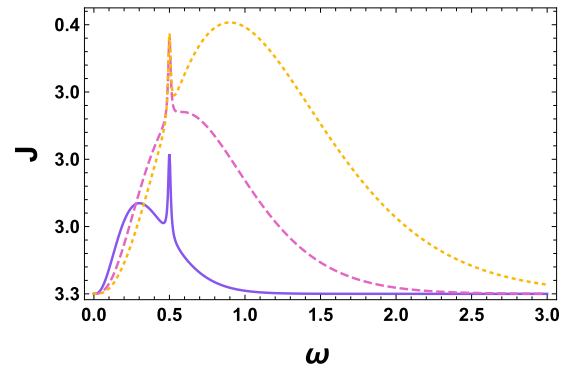


FIG. 1. Normalized spectral density function $J(\omega) = J_{\text{ac}}(\omega) + J_{\text{op}}(\omega)$ for an Einstein optical mode at $\omega_0 = 0.5$ with Lorentzian broadening $\Gamma = 0.01$, and characteristic acoustic phonon frequencies: Purple (solid line) $\omega_c = 0.1$, pink (dashed line) $\omega_c = 0.2$, orange (dotted line) $\omega_c = 0.3$, for $\gamma_{\text{ac}}/\gamma_{\text{op}} = 200$.

spreads over a much larger range than ω_c , and the density of states for the lower frequency modes is severely suppressed as ω_c is increased. The former observation indicates that ω_c is not the actual ‘‘cut-off’’ frequency to the distribution (unlike a Debye frequency which is a physical maximum). This simplified form of the spectral density function, adopted here so that various integrals can be evaluated semianalytically, does limit the extent to which the calculated spectra below can be quantitatively compared to experimental results.

With this $J_{\text{ac}}(\omega)$, the phase at $T = 0$ K is found to be

$$\varphi_{\text{ac}}(t) = \frac{\sqrt{1 + \zeta^2}}{(1 + i\omega_c t)^2} \quad (22)$$

and the contribution to the Debye-Waller factor simplifies to $B_{\text{ac}} = e^{-\sqrt{1 + \zeta^2} \gamma_{\text{ac}}}$.

For the acoustic phonons, the Holstein contribution to the emission spectrum, see Eq. (17), is then calculated to be

$$\begin{aligned} & \text{Re}[\Upsilon_{\text{ac}}^0(\xi - \epsilon_\zeta - i\eta)] \\ & \approx \frac{\eta}{(\xi - \epsilon_\zeta)^2 + \eta^2} + \frac{\gamma}{\omega_c^2} B_0^2 \exp\left(\frac{\xi - \epsilon_\zeta}{\omega_c}\right) \\ & \quad \times \cos\left(\frac{\eta}{\omega_c}\right) (\xi - \epsilon_\zeta) \theta(\epsilon_\zeta - \xi) + \frac{\gamma^2}{12\omega_c^4} \\ & \quad \times B_0^2 \exp\left(\frac{\xi - \epsilon_\zeta}{\omega_c}\right) \cos\left(\frac{\eta}{\omega_c}\right) (\xi - \epsilon_\zeta)^3 \theta(\epsilon_\zeta - \xi) \end{aligned} \quad (23)$$

while the corresponding expression for the Peierls contribution is listed in Appendix C.

B. Optical phonons

In addition to low-momentum acoustic phonon with linear dispersion modeled by the $J_{\text{ac}}(\omega)$, experimentally determined phonon spectra for semiconductors such as silicon also reveal dispersionless optical phonons at low momenta, as well as flat portions of some acoustic phonon branches near the BZ boundary [6,23]. For small enough ranges of momenta, such flat portions of the dispersion curves can be modeled as Einstein modes, leading to contributions of the form $J_{\text{op}}(\omega) = \gamma_{\text{op}} \omega_0^2 \delta(\omega - \omega_0)$ where γ_{op} is the dimensionless coupling

TABLE I. Summary of model parameters used and their physical description.

ϵ	Optical transition energy/TLS transition energy
ζ	Peierls coupling strength (dimensionless)
ω_c	Characteristic acoustic phonon frequency
ω_0	Optical (Einstein) phonon frequency
γ_{ac}	Acoustic phonon coupling strength (dimensionless)
γ_{op}	Optical phonon coupling strength (dimensionless)
η	Phenomenological damping
Γ	Optical phonon linewidth

strength of this constant energy mode. In Fig. 1 we plot such a contribution for $\omega_0 = 0.5$, where the δ function is replaced by a Lorentzian with a broadening $\Gamma = 0.01$.

The coupled phonon propagator is easily evaluated for such $J_{op}(\omega)$ to be $\varphi_{op}(t) = \sqrt{1 + \zeta^2} \gamma_{op} \exp(-i\omega_0 t)$ and the corresponding contribution to the Debye-Waller factor is $B_{op} = e^{-\sqrt{1 + \zeta^2} \gamma_{op}}$.

The corresponding contribution to the emission spectrum from optical phonons is then just a Lorentzian $\Upsilon_{op}(\xi - \epsilon_\zeta) = \gamma_{op} \Gamma / [(\xi - \epsilon_\zeta)^2 + \Gamma^2]$, with half-width half-maximum Γ . Taylor expansion of $e^{\varphi_{ac} + \varphi_{op}}$ to second order in electron-phonon couplings also produces a mixed term $\Upsilon_{mix}(\xi)$ (listed in Appendix C) accounting for simultaneous acoustic and optical phonons emission.

Table I provides a summary of the various parameters introduced in this model, and their physical associations.

The strength of the electron-phonon coupling can be directly linked to the number of phonons in the cloud. In the ground state, for Holstein-only coupling, this corresponds to $\langle n \rangle = \sum_q u_q^2 / 4 = \int d\omega J(\omega) / 4\omega^2$. For example, for the simplistic optical phonon spectral density we consider here, this evaluates to $\langle n \rangle = \gamma_{op} / 4$. This is reflected in the fact that the difference in the number of phonons in the optical transitions excited and ground state's clouds is an indication of the amount of spectral weight that is removed from the optical transition and goes into the phonon sideband. The Debye-Waller factor is closely related to this quantity, as can be seen by expansion of Eq. (16). We will show in Sec. IV that the Peierls coupling, at least within our approximation of small ζ , has very little effect on this quantity but instead substantially alters the lifetime of the optical transition.

IV. RESULTS

We are now ready to calculate the emission spectrum of Eq. (17) for various cases. For completeness, we first consider the pure Holstein contribution to the emission spectrum if there are only acoustic phonons, such that $\varphi(t) = \varphi_{ac}(t)$. Figure 2 illustrates the effect of increasing the dimensionless coupling γ_{ac} . For $\gamma_{ac} = 0$, only the ZPL is present in the spectrum, with a linewidth entirely due to the phenomenological broadening η . The broad shape of the phonon sideband visible at finite γ_{ac} can be attributed to the acoustic phonon spectral density function used, which is peaked towards the lower frequencies (relative to the ZPL) and presents a broad tail owing to the small, but nevertheless significant spectral weight at high frequencies, controlled by the parameter ω_c .

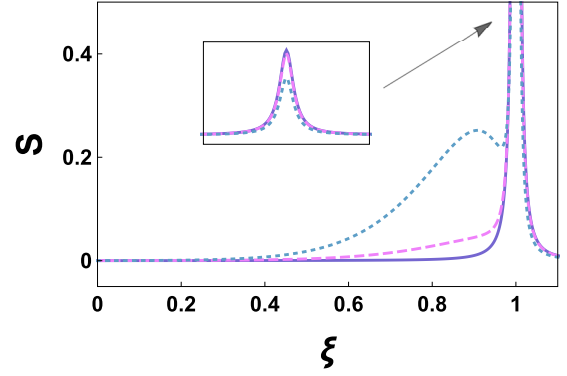


FIG. 2. Emission spectrum for the pure Holstein model ($\zeta = 0$) with acoustic phonons only. We set $\epsilon = 1$ as our energy unit. Other parameters are $\omega_c = 0.1$, $\eta = 0.0001$. The dimensionless coupling strength is: purple (solid line) $\gamma_{ac} = 0$, pink (dashed line) $\gamma_{ac} = 0.01$, and blue (dotted line) $\gamma_{ac} = 0.1$.

As γ_{ac} is switched on we see the formation of a continuous phonon sideband, as phonon emission becomes more likely. For $\gamma_{ac} = 0.1$, the phonon sideband already contains significant spectral weight, corresponding in a reduction of the ZPL spectral weight (see inset), reflecting the decreasing likelihood of the optical transition relaxation without a phonon. The broadening of the ZPL peak is still η , i.e., there is no additional broadening due to Holstein coupling to phonons.

Next, we turn on the Peierls electron-phonon coupling $\zeta \neq 0$ and calculate the corresponding emission spectrum, this time with an added optical phonon mode at $\omega_0 = 0.1$, such that $\varphi(t) = \varphi_{ac}(t) + \varphi_{op}(t)$. The corresponding emission spectrum is shown in Fig. 3. For $\zeta = 0$ (solid blue line), we recover the Holstein-only coupling but now with additional sideband peaks at energies $\xi = \epsilon - n\omega_0$. For this coupling strength, only the $n = 1, 2$ peaks are resolved due to the models' second order perturbative treatment of the electron-phonon coupling. This reflects the fact that the strength of the electron-phonon coupling represents the number of phonons in the cloud thereby capping the number of optical phonon peaks at two.

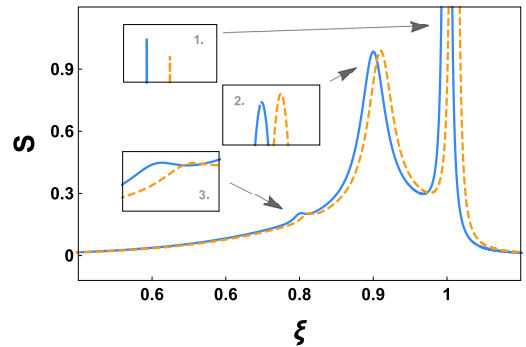


FIG. 3. Emission spectrum for dual coupling to acoustic phonons and an optical phonon mode. Inset 1: ZPL, inset 2: first order optical phonon peak, inset 3: second order optical phonon peak. The parameters are $\epsilon = 1$, $\omega_c = 0.1$, $\omega_0 = 0.1$, $\gamma_{ac} = 0.1$, $\gamma_{op} = 0.05$, $\eta = 0.0001$, $\Gamma = 0.01$. The relative strength of the Peierls coupling is blue (solid line) $\zeta = 0$, and orange (dashed line) $\zeta = 0.1$.

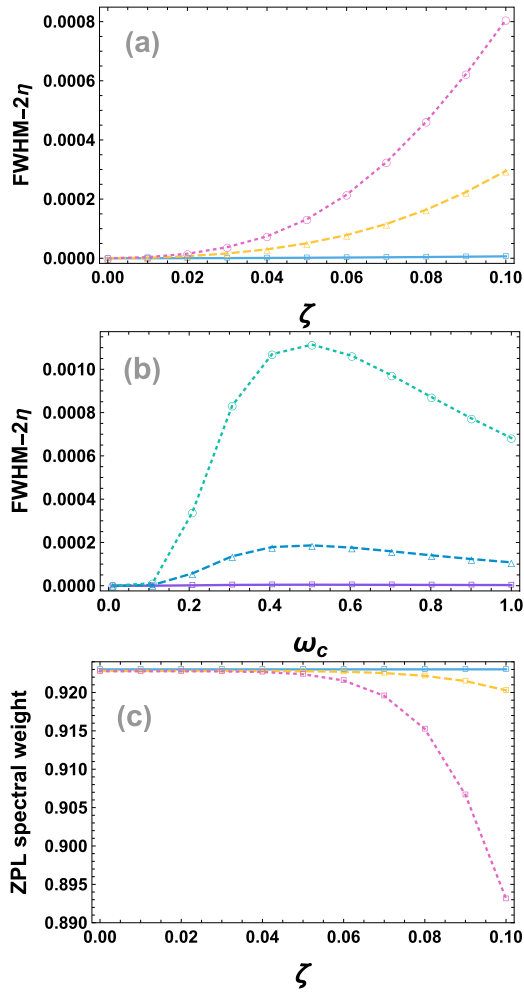


FIG. 4. ZPL characteristics in the presence of Peierls coupling to acoustic phonons only: $J(\omega) = J_{ac}(\omega)$. (a) Full-width half-maximum (FWHM) vs ζ , for $\omega_c = 0.1$ (blue squares), $\omega_c = 0.2$ (yellow triangles), and $\omega_c = 0.3$ (pink circles). (b) FWHM vs ω_c , for $\zeta = 0.01$ (purple squares), $\zeta = 0.05$ (blue triangles), and $\zeta = 0.1$ (green circles). (c) ZPL spectral weight relative to total spectral weight [same legend as (a)]. Other parameters are $\epsilon = 1$, $\gamma_{ac} = 0.1$, $\eta = 0.0001$.

When ζ is switched on (orange dashed line), we note two effects of the Peierls coupling on both the ZPL and phonon sideband. The first is a frequency shift to the entire spectrum (ZPL and sideband) arising from the renormalization of the optical transition frequency, see Eq. (4). The second is a reduction in ZPL peak height alongside an increased weight in the phonon sideband, as shown in the insets, qualitatively similar to Fig. 2.

More careful inspection of the ZPL reveals a third, *qualitatively new effect* produced by the Peierls coupling on the emission spectrum. To illustrate it, we fit the ZPL with a Lorentzian and extract its full-width half-maximum (FWHM) and fraction of the total integrated spectral weight. The results are plotted in Fig. 4.

Figure 4(a) shows that unlike for pure Holstein coupling, in the presence of Peierls coupling $\zeta \neq 0$, the ZPL acquires a finite intrinsic broadening in addition to the phenomenological η . This can be a substantial effect, with a intrinsic broadening

of as much as 0.2% of the ZPL energy for $\gamma_{ac} = 0.1$, $\zeta = 0.1$, and $\omega_c = 0.3$. The ZPL broadening is also seen to depend strongly on the characteristic acoustic phonon frequency ω_c [see Fig. 4(b)] indicating the importance of the distribution of phonon modes in the bath. Along with this increasing broadening, the ZPL spectral weight diminishes with ζ [Fig. 4(c)], indicating that phonon-assisted emission becomes more likely with increased Peierls coupling. The spectral weight distribution between ZPL and sideband can also be inferred from this plot where we see that the ZPL dominates over the sideband, at least within the range of parameters used for our model. The relative low intensity of the sideband feature is due to the small electron-phonon coupling strengths used and would be amplified for stronger couplings. For real systems, such as the $\text{Se}^+:\text{Si}$ system we consider in Sec. IV, experimentalists are able to probe these sideband features despite their relative low intensities, as there is no significant background noise beyond phonon excitations [22].

The origin of the ZPL broadening induced by the Peierls coupling can be understood as follows. If we consider the Holstein-only coupling contribution to the Hamiltonian, we recover the well-known, exactly solvable, independent Boson (IB) model [32]. The corresponding spectrum has two manifolds corresponding to the two possible impurity spin projections $\sigma = |1\rangle, |2\rangle$ (see Appendix D for details). Phonon emission due to Holstein coupling conserves the spin, hence it cannot induce a transition between any states belonging to the two different manifolds. This is why Holstein-only coupling does not lead to an intrinsic broadening of the ZPL.

By contrast, a Peierls coupling allows for such transitions, thereby inducing a finite lifetime to the excited dipole transition. To demonstrate this explicitly, we treat the Peierls coupling as a perturbation and apply FGR to calculate the decay rate of an initially excited optical transition. This predicts the excited state inverse lifetime to increase quadratically with Peierls coupling ζ and to have a nonmonotonic dependence of ω_c [see Eq. (E2)], in strong agreement with the linewidth calculated from $S(\xi)$ and shown in Fig. 4. The details are discussed in Appendix D.

We now turn our attention to address the relevance of these model calculations to experimental measurements in the specific cases of phosphorous and selenium donor impurities in silicon. Both of these impurities exhibit long spin lifetimes in isotopically purified silicon, making them attractive as spin qubits [2]. Spin-photon coupling at microwave ($\epsilon = 34$ meV) and mid infrared ($\epsilon = 427$ meV) [22,35] frequencies, respectively, may offer a means of coupling adjacent spin qubits [22].

The T_1 contribution to the ZPL linewidth of the phosphorous $1S-2P_o$ TLS transition is ~ 1.5 μeV [21]. In our model, the ZPL linewidth is due entirely to T_1 processes and to first order it is determined entirely by the phonon spectral function evaluated at $\epsilon = 34$ meV and ζ . To second order, the detailed shape of the spectral function will play a role. Since the phonon density of states of silicon has a large peak near 34 meV, we choose an analytic approximation to the relevant spectral function to comprise a continuum parametrized by $\omega_c = 5$ meV, plus an optical phonon mode parametrized by an ω_o that can be varied about 34 meV. Figure 5 shows the prediction for the ZPL linewidth (a proxy for the inverse T_1

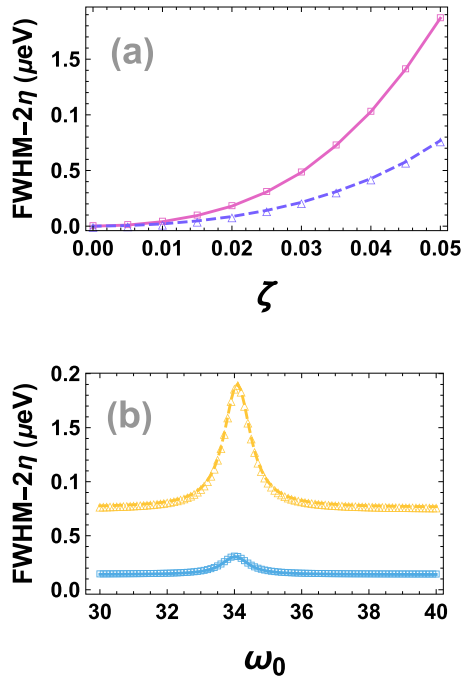


FIG. 5. Change in FWHM of the P:Si model ZPL. Parameters are $\epsilon = 34$ meV, $\omega_c = 5$ meV, $\gamma_{ac} = 0.1$, $\gamma_{op} = 0.001$, $\eta = 0.5$ μ eV. (a) Pink: $\omega_0 = 34$ meV, purple: $\omega_0 = 40$ meV, (b) blue: $\zeta = 0.025$, yellow: $\zeta = 0.05$.

time) as a function of ζ for a set of ω_0 values. The ZPL transition contributes ~ 0.6 to the entire spectrum in these calculations, regardless of the value of ω_0 .

The experimental T_1 limited ZPL linewidth of ~ 1.5 μ eV can therefore be obtained from the model calculations either assuming a moderate Peierls coupling to a resonant “optical” phonon mode (really here the optical mode mimics a flat portion of the acoustic spectrum), or by increasing the Peierls coupling if the spectral function is not strongly peaked at 34 meV. Regardless of this tradeoff, model values of ζ on the order of 5% seem consistent with the experimental value.

In the case of Se, there is negligible ZPL linewidth predicted by the model because it would take at least seven phonons to induce a transition at this large ϵ . However, the fluorescence emission spectrum and the relative ZPL spectral weight have been measured at cryogenic temperatures [22]. In Fig. 6 we plot the emission spectrum calculated for this optical transition (solid line), using the same phonon spectral density functions used for the P calculations, with the addition of two optical phonon modes at 18 and 55 meV to better reflect the triple peaked phonon density of states in silicon that does manifest itself in the experimental sideband spectra. The model parameters γ_{ac} , γ_{op} , ω_c , Γ , ω_0 were adjusted within the bounds imposed by the approximations used in our formalism, to generate a phonon sideband spectrum that comes closest to that experimentally reported [22]. However, it is important to note that we have to limit the upper values of the ζ , γ_{ac} , and γ_{op} parameters because our analytic calculations are only expected to be accurate for weak couplings.

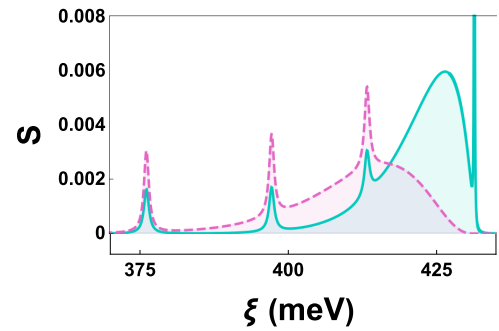


FIG. 6. Emission spectrum at zero temperature for the Se:Si optical transition (green line) for the phonon spectral density function $J(\omega)$ (pink dashed line). Parameters are $\epsilon = 427$ meV, $\omega_c = 5$ meV, three optical phonons at: $\omega_1 = 18$ meV, $\omega_2 = 34$ meV, $\omega_3 = 55$ meV, $\gamma_{ac} = 0.1$, $\gamma_{op} = 0.001$, $\eta = 0.1$ μ eV, $\Gamma = 0.5$, $\zeta = 0.1$.

The calculated sideband spectrum only vaguely resembles that measured in experiments: the shape does not include a large enough contribution from the continuum, and the ZPL line in Fig. 6 represents 87% of the total spectral weight of the emission spectrum, substantially larger than the 16% observed in experiment (this outcome is not significantly changed by varying ζ). Both of these deficiencies suggest that the electron-phonon coupling strength is likely larger than can be accounted for with the current approximations. Clearly a better model for $J(\omega)$ and a numerical evaluation of the various integrals will be necessary to obtain a more accurate agreement, however we can conclude that the current model Hamiltonian that includes both diagonal and off-diagonal coupling provides a semiquantitative description of the experimental sideband spectral shape, and the relative ZPL spectral weight.

V. SUMMARY AND CONCLUSIONS

We have analyzed a model that studies the emission/absorption properties of a dipole optical transition subject to both Holstein (diagonal) and Peierls (nondiagonal) electron-phonon coupling. Our analysis was performed entirely analytically, using the powerful non-Markovian method of NIBA, which retains feedback mechanisms from the phonon bath.

Our results demonstrate the sensitivity of the characteristics of these optical transitions not only to the strength of the electron-phonon coupling—especially the Peierls coupling—but also to parameters pertaining to the distribution of phonon modes in the environment. We find that both forms of coupling enhance phonon sideband formation in the emission spectra, however *only* the Peierls coupling also leads to linewidth broadening of the ZPL, in contrast to the infinite lifetime obtained for Holstein-only coupling. This demonstrates the importance of including Peierls couplings for realistic studies of these systems. The resulting excited state lifetimes are found to depend strongly on the distribution of phonon modes in the environment, with phonon spectral densities favoring a low-frequency distribution of modes producing

much longer lifetimes than those peaked towards higher frequencies.

It is important to note that these calculations were performed at zero temperature, so this Peierls induced broadening is entirely due to quantum fluctuations. At finite temperatures we expect to see an additional temperature dependent broadening.

Both the simplified analytic form of the spectral density function assumed in these calculation, and the limitations on the diagonal and off-diagonal coupling strengths imposed by the model approximations, limit the extent to which direct comparisons with experimental results can be made. Nevertheless, in the case of the ZPL linewidth of P, it appears a Peierls parameter on the order of 5% is required for the model to reproduce experimental results. In the case of the Se emission spectrum in silicon, the results suggest that the model likely has to be extended to allow for at least one order higher (third order) in the Holstein phonon coupling strength.

Further work will therefore include extending the approximations to higher order in the coupling strengths, and using more realistic spectral density functions. The results should help guide the search for materials and defect centers that offer the desired optical properties to complement long spin-coherence lifetimes, for high-fidelity spin-photon interface applications in quantum information applications.

ACKNOWLEDGMENTS

We gratefully acknowledge financial support from the Grand Challenges research program at the Stewart Blusson Quantum Matter Institute, the Natural Sciences and Engineering Research Council, and the Canada First Research Excellence Fund.

APPENDIX A: ELECTRON-PHONON COUPLING TO A DEFECT DIPOLE TRANSITION

Defect spin qubits are generally associated with an electronic spin degree of freedom and are not usually affected by electron-phonon coupling. However, in order to experimentally access the spin qubit state, an optical transition associated with some other levels within the ground and excited state manifolds of the defect atom are often utilized. See Ref. [1] for the specific case of selenium atoms in silicon. The dipole transition is however subject to electron-phonon coupling and we briefly outline the physical origin of this coupling below.

Donor atoms placed inside a semiconductor host lattice like silicon are pointlike defects in the lattice, whereas the bound electron wave function extends across many lattice sites. As a result, the energy level structure of the donor atom is significantly modified by the host lattice. In the case of silicon for example, the sixfold valley degeneracy leads to valley-orbit splitting and the excited states of the donor atom will become linear combinations of wave functions associated with the six equivalent valleys [36], specifically: $\phi_\sigma(\vec{r}) = \sum_{\lambda=1}^6 \chi_{\sigma,\lambda} u_\lambda(\vec{r})$. Here $\sigma = 1, 2$ is the pseudospin index, $\lambda = 1 - 6$ are the valleys, and $u_\lambda(\vec{r})$ are their individual

contributions, while $\chi_{\sigma,\lambda} = \pm 1$ define the symmetry of the linear combination.

Coupling to phonons arises from modulations of the electron-ion interaction $\sum_n V(\vec{r} - \vec{R}_n) = \sum_n V(\vec{r} - \vec{R}_n^{(0)}) - \sum_n \vec{u}_n \nabla V(\vec{r} - \vec{R}_n^{(0)})$. Here n indexes ions, $\vec{R}_n^{(0)}$ are their equilibrium positions, and \vec{u}_n are their displacements from equilibrium which can be expanded in terms of phonon operators. Finite off-diagonal coupling arises if the matrix elements $\langle \phi_\uparrow | \nabla V(\vec{r} - \vec{R}_n^{(0)}) | \phi_\downarrow \rangle \neq 0$. Up to (noncanceling) signs arising from the product of the various χ , these matrix elements have contributions similar to those for the diagonal coupling $\langle \phi_\uparrow | \nabla V(\vec{r} - \vec{R}_n^{(0)}) | \phi_\uparrow \rangle - \langle \phi_\downarrow | \nabla V(\vec{r} - \vec{R}_n^{(0)}) | \phi_\downarrow \rangle \neq 0$.

This is the origin of electron-phonon interactions for defect atoms in semiconductor environments, however it should be noted that the Hamiltonian we consider in this work is quite general and is not necessarily restricted to this situation.

APPENDIX B: FLUORESCENCE EMISSION SPECTRUM IN THE POLARON FRAME AND INTERACTION PICTURE

The fluorescence spectrum of emitted radiation by an oscillating dipole source in a thermal equilibrium state at $t = 0$ is given by Eq. (9) in the main text. Performing the trace over the spin degrees of freedom, one is left with the matrix element

$$S(\xi') = \text{Re} \int_0^\infty dt e^{-i\xi't} \langle \langle 1 | \sigma_-(t) | 2 \rangle \rangle_{\text{ph}} \quad (\text{B1})$$

as the spin space is restricted to $\{|1\rangle = |\downarrow\rangle, |2\rangle = |\uparrow\rangle\}$ and the system is initialized in the state $|2\rangle = \sigma_+(0) |1\rangle$, and we need to perform the trace over the phonon bath $\langle \dots \rangle_{\text{ph}} = \text{tr}_{\text{ph}}(\dots)$.

Transforming to the polaron frame we insert the identity $\mathbb{1} = \tilde{U} \tilde{U}^\dagger$, see Eq. (2):

$$S(\xi') = \text{Re} \int_0^\infty dt e^{-i\xi't} \langle \langle 1 | \tilde{U} \tilde{\sigma}_-(t) \tilde{U}^\dagger | 2 \rangle \rangle_{\text{ph}}, \quad (\text{B2})$$

where $\tilde{\sigma}_-(t) = \tilde{U}^\dagger \sigma_- \tilde{U}$ is now in the polaron frame. Expanding $\tilde{U} = \mathbb{1} - (\sigma_z + \zeta \sigma_x) \sum_q u_q (b_q - b_q^\dagger) + \frac{1}{2!} (\mathbb{1} + \zeta^2 \sigma_x) \sum_q u_q^2 (b_q - b_q^\dagger)^2 + \dots$ and collecting terms, we find: $\langle 1 | \tilde{\sigma}_-(t) | 2 \rangle = \langle 1 | e^{\hat{\phi}_0} \tilde{\sigma}_-(t) e^{-\hat{\phi}_0} | 2 \rangle + \langle 1 | e^{\hat{\phi}_0} \tilde{\sigma}_-(t) (e^{-\zeta \hat{\phi}_0} - 1) | 1 \rangle + \langle 2 | (e^{\zeta \hat{\phi}_0} - 1) \tilde{\sigma}_-(t) e^{-\hat{\phi}_0} | 2 \rangle + \langle 2 | (e^{\zeta \hat{\phi}_0} - 1) \tilde{\sigma}_-(t) (e^{-\zeta \hat{\phi}_0} - 1) | 1 \rangle$, where $\hat{\phi}_0 = \hat{\phi}(\zeta = 0)$ are as defined in the main text. For convenience, we define $|\tilde{\alpha}\rangle = e^{-\hat{\phi}_0} |\alpha\rangle$, $|\tilde{\alpha}\rangle_\zeta = (e^{-\zeta \hat{\phi}_0} - 1) |\alpha\rangle$ to represent the polaron wave functions.

Next, we move to the interaction picture. Until here, the spin operators in $S(\xi)$ evolve in the Heisenberg picture according to $\sigma_\pm(t) = U_H^\dagger(t) \sigma_\pm U_H(t)$ where $U_H(t) = e^{-i\tilde{H}t}$ and the Hamiltonian $\tilde{H} = \tilde{H}_0 + \tilde{H}'$ is the full Hamiltonian in the polaron frame including its static part \tilde{H}_0 and time-dependent part \tilde{H}' , as defined in the main text.

Consider now the first term in the equation above. In the interaction picture, it becomes $\langle \tilde{1} | \tilde{\sigma}_-(t) | \tilde{2} \rangle = \langle \tilde{1} | e^{i\tilde{H}'t} \tilde{\sigma}'_-(t) e^{-i\tilde{H}'t} | \tilde{2} \rangle = \sum_{\alpha,\beta} \tilde{G}_{\alpha 1}^\dagger(t) \langle \tilde{\alpha} | \sigma'_-(t) | \tilde{\beta} \rangle \tilde{G}_{\beta 2}(t)$, where the spin operators are now in the interaction picture: $\sigma'_\pm(t) = e^{i\tilde{H}_0 t} \sigma_\pm e^{-i\tilde{H}_0 t}$ and we use matrix elements of the propagators $\tilde{G}_{\alpha\beta} = \langle \tilde{\alpha} | e^{-i\tilde{H}'t} | \tilde{\beta} \rangle$.

Treating all other terms similarly, we arrive at the expression for the full emission spectrum:

$$S(\xi') = \text{Re} \int_0^\infty dt e^{-i(\xi' - \epsilon_\zeta)t} [\langle \tilde{G}_{11}^\dagger \tilde{G}_{22} \rangle_{\text{ph}} + \langle \tilde{G}_{11}^\dagger \tilde{G}_{21_\zeta} \rangle_{\text{ph}} + \langle \tilde{G}_{2_\zeta 1}^\dagger \tilde{G}_{22} \rangle_{\text{ph}} + \langle \tilde{G}_{2_\zeta 1}^\dagger \tilde{G}_{11_\zeta} \rangle_{\text{ph}}]. \quad (\text{B3})$$

Performing the time series expansion of the Green's functions, see Eq. (12), reveals that the last three terms in Eq. (B3) produce imaginary first order terms and all subsequent terms are of order $O(\zeta^3) \rightarrow 0$ or higher. Therefore, to this order, the emission spectrum equals

$$S(\xi) \approx \text{Re} \int_0^\infty dt e^{-i\xi t} \langle \tilde{G}_{11}^\dagger(t) \tilde{G}_{22}(t) \rangle_{\text{ph}}. \quad (\text{B4})$$

APPENDIX C: PHONON SPECTRAL DENSITY FUNCTION

Here we describe in more detail the derivation of the cubic form of the acoustic phonon spectral density function, used in the text.

We use the Debye approximation for the acoustic phonon dispersion: $\omega_{s,q} \approx v_s |\mathbf{q}|$ where the index s runs over longitudinal and transverse branches and v is the sound velocity. The spectral density function, defined as $J(\omega) = \sum_{s,q} \lambda_{s,q}^2 \delta(\omega - \omega_{s,q})$, contains a summation over each branch and all the momenta in the Brillouin zone, which is taken to be a sphere of radius q_D . In the thermodynamic limit we replace $\sum_{s,q} \dots \rightarrow \sum_s \int_0^{q_D} dq q^2 \dots$ (up to normalization factors). Finally, we consider the deformation potential for electron scattering by acoustic phonons, where the coupling is found to be [32,37]

$$\lambda_{s,q} = \frac{2\kappa_s q}{\sqrt{2V} \rho \omega_{s,q}}, \quad (\text{C1})$$

where κ is the deformation potential, V is the sample volume, and ρ its mass density.

Inserting everything into $J(\omega)$, performing the integrals, and summing over two transverse and one longitudinal

acoustic phonon branches produces [38,39]

$$J_{\text{ac}}(\omega) = \left(\frac{\kappa_l^2}{v_l^5} + \frac{2\kappa_t^2}{v_t^5} \right) \frac{\omega^3}{2\pi\rho}, \quad (\text{C2})$$

where the material constants are customarily grouped into $\gamma_{\text{ac}}/\omega_c^2$.

APPENDIX D: THE TWO-POINT PHONON CLOUD CORRELATION FUNCTION

In truncating the number of long-range (in time) phonon cloud processes according to NIBA we are left with calculating a two-point correlation function that describes interacting successive bath displacements:

$$\begin{aligned} & \langle \hat{K}_+(t) \hat{K}_-(t') \rangle_{\text{ph}} \\ &= \left\langle \frac{(\zeta\epsilon)^2}{4(1+\zeta^2)^2} (\cosh[\hat{\phi}_\zeta(t)] - 1)(\cosh[\hat{\phi}_\zeta(t')] - 1) \right. \\ & \quad - \frac{(\zeta\epsilon)^2}{4(1+\zeta^2)} \sinh[\hat{\phi}_\zeta(t)] \sinh[\hat{\phi}_\zeta(t')] \\ & \quad - \frac{(\zeta\epsilon)^2}{4(1+\zeta^2)^{\frac{3}{2}}} (\cosh[\hat{\phi}_\zeta(t)] - 1) \sinh[\hat{\phi}_\zeta(t')] \\ & \quad \left. + \frac{(\zeta\epsilon)^2}{4(1+\zeta^2)^{\frac{3}{2}}} (\cosh[\hat{\phi}_\zeta(t')] - 1) \sinh[\hat{\phi}_\zeta(t)] \right\rangle_{\text{ph}}. \quad (\text{D1}) \end{aligned}$$

Expanding the hyperbolic functions in terms of the bath displacement operators $e^{\hat{\phi}_\zeta(t)}$ and $e^{-\hat{\phi}_\zeta(t)}$, we obtain a combination of two-point correlation functions of the form $\langle \hat{B}_\pm(t) \hat{B}_\mp(t') \rangle_{\text{ph}} = B^2 \langle e^{\pm\hat{\phi}_\zeta(t)} e^{\mp\hat{\phi}_\zeta(t')} \rangle_{\text{ph}}$, $\langle \hat{B}_\pm(t) \hat{B}_\pm(t') \rangle_{\text{ph}} = B^2 \langle e^{\pm\hat{\phi}_\zeta(t)} e^{\pm\hat{\phi}_\zeta(t')} \rangle_{\text{ph}}$, as well as Debye-Waller factors B given by Eq. (16).

For Holstein (diagonal) coupling, the two-point phonon cloud correlation functions are well known [29,32]:

$$\langle \hat{B}_\pm(t) \hat{B}_\mp(t') \rangle_{\text{ph}} = B^2 \exp[\varphi(t - t')] \quad (\text{D2})$$

with $\varphi(t)$ defined in the main text in both its discrete and continuous forms, see Eqs. (15) and (19).

It remains to calculate the Fourier transform of the Peierls contribution to the phonon cloud correlation function $\Upsilon(\xi) = \nu(\xi) + \Upsilon_{\text{ac}}(\xi) + \Upsilon_{\text{op}}(\xi) + \Upsilon_{\text{mix}}(\xi)$ defined in Eq. (17). To facilitate this we expand to second order in the phase $\varphi(t)$ to find

$$\nu(\epsilon_\zeta - i\eta) = \frac{(\zeta\epsilon)^2 B_0^2 (1 - 2B)\eta}{2(1 + \zeta^2)^2 (\epsilon_\zeta^2 + \eta^2)}, \quad (\text{D3})$$

$$\begin{aligned} \Upsilon_{\text{ac}}(\epsilon_\zeta - i\eta) &= -\frac{\gamma_{\text{ac}}(\zeta\epsilon)^2 \epsilon_\zeta}{2\omega_c^2 (1 + \zeta^2)} B_0^2 B^2 \exp\left[\frac{-\epsilon_\zeta}{\omega_c}\right] \cos(\eta/\omega_c) \theta(\epsilon_\zeta) + \frac{(\zeta\epsilon)^2}{2(1 + \zeta^2)^2} B_0^2 B^2 \\ & \quad \times \left[\frac{\eta}{\epsilon_\zeta^2 + \eta^2} + \frac{\gamma_{\text{ac}} \epsilon_\zeta}{6\omega_c^4} \exp\left[\frac{-\epsilon_\zeta}{\omega_c}\right] \cos(\eta/\omega_c) 3\eta^2 (1 - \epsilon_\zeta^2) \theta(\epsilon_\zeta) \right], \\ \Upsilon_{\text{op}}(\epsilon_\zeta - i\eta) &= -\frac{\gamma_{\text{op}} B_0^2 B^2 (\zeta\epsilon)^2 \Gamma}{(1 + \zeta^2)[(\omega_0 - \epsilon_\zeta)^2 + \Gamma^2]}, \\ \Upsilon_{\text{mix}}(\epsilon_\zeta - i\eta) &= \frac{\gamma_{\text{ac}} \gamma_{\text{op}} (\zeta\epsilon)^2 B_0^2 B^2 \exp\left[\frac{\omega_0 - \epsilon_\zeta}{\omega_c}\right]}{\omega_c^2 (1 + \zeta^2)^2} \theta(\epsilon_\zeta) \left[(\epsilon_\zeta - \omega_0) \cos\left(\frac{\Gamma + \eta}{\omega_c}\right) + (\Gamma + \eta) \sin\left(\frac{\Gamma + \eta}{\omega_c}\right) \right], \quad (\text{D4}) \end{aligned}$$

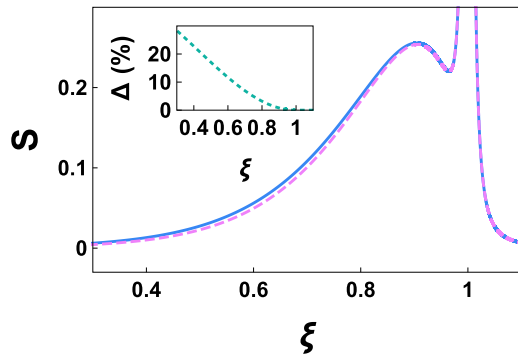


FIG. 7. Comparison of emission spectrum predicted by formalism used in the main text (blue solid line) and perturbation theory (pink dashed line) for a pure Holstein-coupling ($\zeta = 0$) model with acoustic phonons. Inset shows percentage difference between model and perturbation theory results. Parameters are $\epsilon = 1$, $\gamma_{ac} = 0.1$, $\omega_c = 0.1$, $\eta = 0.0001$.

where the real part has been retained only as required by Eq. (10).

APPENDIX E: PERTURBATION THEORY CALCULATION OF ZPL LINEWIDTH AND SIDEBAND

If we set $\zeta = 0$ in Eq. (1), we recover the well-known IB model. It is exactly solvable and produces two manifolds of eigenstates $|\sigma, \{n_q\}\rangle \equiv |\sigma\rangle \otimes \prod_q \frac{(B_{q\sigma}^\dagger)^{n_q}}{\sqrt{n_q!}} |\sigma u\rangle$, where $\sigma = \pm$ labels the spin's eigenstates, the dressed phonon operators are $B_{q\sigma} = b_q - \sigma u_q/2$, and their corresponding vacuum states are $|\sigma u\rangle = \prod_q e^{-u_q^2/2 + \sigma u_q b_q^\dagger} |0\rangle$. Their corresponding eigenenergies are $E_{\sigma, \{n_q\}} = \sigma \frac{\epsilon}{2} - \sum_q \lambda_q^2/4\omega_q + \sum_q \omega_q n_q$.

Using perturbation theory, we calculate the corresponding emission spectrum to be

$$S(\xi) = e^{-\gamma_{ac}} [\pi \delta(\epsilon - \xi) + \frac{\gamma_{ac}}{\omega_c^2} (\epsilon - \xi) e^{-(\epsilon - \xi)/\omega_c}], \quad (\text{E1})$$

where the first term is the infinite lifetime ZPL and the second one is the phonon sideband. In Fig. 7 we compare $S(\xi)$ calculated using the polaron transformation technique outlined in the main text (for $\zeta = 0$), to this first order PT result in Eq. (E1). For low-phonon frequencies both methods agree

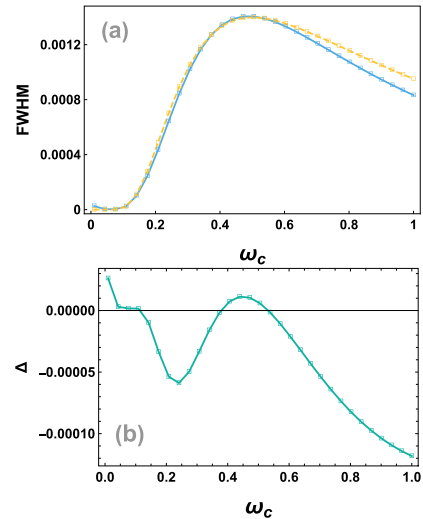


FIG. 8. Comparison of ZPL FWHM for model (blue solid line) and perturbation theory (PT) results (yellow dashed line) for $\gamma = 0.1$ (a). Difference between FWHM calculated from $S(\xi)$ and PT (b). Measured relative to $\eta = 0.001$ (in units of ϵ).

well, as expected, but begin to diverge for higher frequencies as higher order processes (underestimated by first order PT theory) come into effect. The inset shows the percent difference between $S(\xi)$ for both methods.

We can also calculate the transition probability for a system prepared initially in the state $|\sigma = |2\rangle, \{0\}\rangle$, to decay into the continuum of states $|\sigma = |1\rangle, \{n_q\}\rangle$, through Peierls coupling. Using FGR, the rate of decay (proportional to the inverse lifetime τ) is

$$\frac{1}{\tau} = \gamma_{ac} \zeta^2 \frac{\pi \epsilon^3}{2\omega_c^2} e^{-2\gamma_{ac} - \epsilon/\omega_c}. \quad (\text{E2})$$

The corresponding $\text{FWHM} = 2/\tau$ is compared in Fig. 8 to the linewidths extracted from $S(\xi)$ using the fitting procedure outlined in the main text. We find very good agreement between the two methods, comparing their functional dependencies on ω_c [Fig. 8(a)] and calculating the difference Δ between the two methods in Fig. 8(b).

[1] K. J. Morse, R. J. S. Abraham, A. DeAbreu, C. Bowness, T. S. Richards, H. Riemann, N. V. Abrosimov, P. Becker, H. J. Pohl, M. W. Thewalt, and S. Simmons, *Sci. Adv.* **3**, e1700930 (2017).
 [2] K. Saeedi, S. Simmons, J. Z. Salvail, P. Dluhy, H. Riemann, N. V. Abrosimov, P. Becker, H. Pohl, J. J. L. Morton, and M. L. W. Thewalt, *Science* **342**, 830 (2013).
 [3] G. Wolfowicz, A. M. Tyryshkin, R. E. George, H. Riemann, N. V. Abrosimov, P. Becker, H. Pohl, M. L. W. Thewalt, S. A. Lyon, and J. J. L. Morton, *Nat. Nanotechnol.* **8**, 561 (2013).
 [4] K. Nemoto, M. Trupke, S. J. Devitt, A. M. Stephens, B. Scharfenberger, K. Buczak, T. Nobauer, M. S. Everitt, J. Schmiedmayer, and W. J. Munro, *Phys. Rev. X* **4**, 031022 (2014).

[5] X. Yan, S. Gitt, B. Lin, D. Witt, M. Abdolahi, A. Afifi, A. Azem, A. Darcie, J. Wu, K. Awan, M. Mitchell, A. Pfenning, L. Chrostowski, and J. Young, *APL Photonics* **6**, 070901 (2021).
 [6] E. Jánzén, G. Grossmann, R. Stedman, and H. G. Grimmeiss, *Phys. Rev. B* **31**, 8000 (1985).
 [7] J. L. O'Brien, *Science* **318**, 1567 (2007).
 [8] T. Holstein, *Ann. Phys.* **8**, 343 (1959).
 [9] K. Roy-Choudhury and S. Hughes, *Phys. Rev. B* **92**, 205406 (2015).
 [10] K. Roy-Choudhury and S. Hughes, *Optica* **2**, 434 (2015).
 [11] E. V. Denning, J. Iles-Smith, N. Gregersen, and J. Mork, *Opt. Mater. Express* **10**, 222 (2020).

- [12] A. J. Leggett, S. Chakravarty, A. T. Dorsey, M. P. A. Fisher, A. Garg, and W. Zwerger, *Rev. Mod. Phys.* **59**, 1 (1987).
- [13] R. Peierls, *Quantum Theory of Solids* (Clarendon, Oxford, 1955).
- [14] D. J. J. Marchand, P. C. E. Stamp, and M. Berciu, *Phys. Rev. B* **95**, 035117 (2017).
- [15] V. M. Stojanovic, P. A. Bobbert, and M. A. J. Michels, *Phys. Rev. B* **69**, 144302 (2004).
- [16] K. Hannewald, V. M. Stojanović, J. M. T. Schellekens, P. A. Bobbert, G. Kresse, and J. Hafner, *Phys. Rev. B* **69**, 075211 (2004).
- [17] R. W. Munn and R. Silbey, *J. Chem. Phys.* **83**, 1843 (1985).
- [18] A. Norambuena, S. A. Reyes, J. Mejía-López, A. Gali, and J. R. Maze, *Phys. Rev. B* **94**, 134305 (2016).
- [19] X. Linpeng, T. Karin, M. V. Durnev, R. Barbour, M. M. Glazov, E. Ya. Sherman, S. P. Watkins, S. Seto, and Kai-Mei C. Fu, *Phys. Rev. B* **94**, 125401 (2016).
- [20] E. A. Muljarov and R. Zimmermann, *Phys. Rev. Lett.* **93**, 237401 (2004).
- [21] P. T. Greenl, S. A. Lynch, A. F. G. van der Meer, B. N. Murdin, C. R. Pidgeon, B. Redlich, N. Q. Vinh, and G. Aeppli, *Nature (London)* **465**, 1057 (2010).
- [22] A. DeAbreu, C. Bowness, R. J. S. Abraham, A. Medvedova, K. J. Morse, H. Riemann, N. V. Abrosimov, P. Becker, H. J. Pohl, M. L. W. Thewalt, and S. Simmons, *Phys. Rev. Applied* **11**, 044036 (2019).
- [23] A. Valentin, J. See, S. Galdin-Retailleau, and P. Dollfus, *J. Phys.: Condens. Matter* **20**, 145213 (2008).
- [24] The bath is just a collection of bosonic modes in Eq. (1) but will be specified as a phonon bath once an appropriate spectral density function is defined.
- [25] A preliminary consideration of this issue based on FGR suggests that inhomogeneous broadening does not suppress broadening. If we include all three types of coupling such that we have $\lambda_{q,x}$, $\lambda_{q,y}$, $\lambda_{q,z}$, then the broadening is proportional to $|\sum_q \frac{\lambda_{q,x} + i\lambda_{q,y}}{\lambda_{q,z}} \omega_q n_q|^2$. Having inhomogeneous couplings will certainly modify the prefactor, but to first order the total broadening is the sum of the broadenings induced separately by the x and the y couplings.
- [26] H. Breuer and F. Petruccione, *The Theory of Open Quantum Systems* (Oxford University Press, Oxford, 2007).
- [27] U. Weiss, *Quantum Dissipative Systems* (World Scientific, Singapore, 2008).
- [28] H. Dekker, *Phys. Rev. A* **35**, 1436 (1987).
- [29] A. Würger, *Phys. Rev. Lett.* **78**, 1759 (1997).
- [30] In the standard literature on the SB model, $\Delta/\omega_c \ll 1$ is considered the relevant limit of validity of the model, where Δ is some intrinsic tunneling frequency to a TLS. Since our problem the transitions between electron states are induced by the coupling to the bath, we consider the corresponding γ/ω_c limit.
- [31] C. Aslangul, N. Pottier, and D. Saint-James, *J. Physique* **47**, 1657 (1986).
- [32] G. Mahan, *Many Particle Physics*, 2nd ed. (Plenum, New York, 1990).
- [33] At finite temperature, the thermal motion of the surrounding lattice atoms produces a further reduction in tunneling rates, characterized by the finite-temperature contribution to the Debye-Waller factor (absent in our calculations).
- [34] The phenomenological damping factor η is necessary for the numerical implementation of the model in the Holstein limit. Furthermore, if we were to include a photon bath in our Hamiltonian—relevant to its application to spin-photon interfaces—then η would physically represent an intrinsic radiation lifetime associated with the coupling to a photonic reservoir.
- [35] H. G. Grimmeiss, E. Janzén, and K. Larsson, *Phys. Rev. B* **25**, 2627 (1982).
- [36] G. Grossman, K. Bergman, and M. Kleverman, *Physica B* **146**, 30 (1987).
- [37] C. Hamaguchi, *Basic Semiconductor Physics* (Springer, Berlin, 2010).
- [38] A. Würger, *J. Phys.: Condens. Matter* **9**, 5543 (1997).
- [39] A. Würger, *Phys. Rev. B* **57**, 347 (1998).